Nuclear Instruments and Methods in Physics Research B 326 (2014) 121–125

Contents lists available at ScienceDirect

Nuclear Instruments and Methods in Physics Research B

journal homepage: www.elsevier.com/locate/nimb

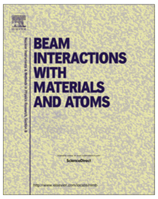

Swift heavy ion-induced phase transformation in Gd_2O_3

Maik Lang [a,*], Fuxiang Zhang [b], Jiaming Zhang [b], Cameron L. Tracy [c], Alex B. Cusick [c], Jason VonEhr [d], Zhiqiang Chen [e], Christina Trautmann [f,g], Rodney C. Ewing [b,c,d]

[a] Department of Nuclear Engineering, University of Tennessee, Knoxville, TN 37996, USA
[b] Department of Earth and Environmental Sciences, University of Michigan, Ann Arbor, MI 48109, USA
[c] Department of Materials Science & Engineering, University of Michigan, Ann Arbor, MI 48109, USA
[d] Department of Nuclear Engineering and Radiological Sciences, University of Michigan, Ann Arbor, MI 48109, USA
[e] Department of Geosciences, SUNY, Stony Brook, NY 11794, USA
[f] GSI Helmholtz Centre for Heavy Ion Research, 64291 Darmstadt, Germany
[g] Technische Universität Darmstadt, 64287 Darmstadt, Germany

ARTICLE INFO

Article history:
Received 1 July 2013
Received in revised form 12 October 2013
Accepted 25 October 2013
Available online 10 February 2014

Keywords:
Swift heavy ions
Sesquioxides
Gd_2O_3
Crystalline-to-crystalline phase transformations
X-ray diffraction

ABSTRACT

Crystalline-to-crystalline phase transformation of cubic Gd_2O_3 induced by swift Au ions with a kinetic energy of 2.25 GeV, has been characterized by synchrotron X-ray diffraction experiments (XRD) as a function of increasing fluence, up to 5×10^{13} ions/cm^2. The diffraction maxima of the initial cubic structure gradually decrease in intensity as function of ion fluence, concurrent with the in-growth of several new diffraction peaks, which, based on Rietveld refinement, correspond to the monoclinic high-temperature phase. The same cubic-to-monoclinic phase transformation induced by swift heavy ions has been observed in Y_2O_3. The transformation pathway under irradiation is consistent with the high-temperature behavior of Gd_2O_3, and is probably associated with a multiple ion-impact mechanism. There was no evidence of amorphous material in the diffraction patterns, even after irradiation to the maximum fluence, at which the initial cubic phase has been completely transformed to the monoclinic structure.

1. Introduction

The radiation response of simple and complex oxides has been extensively studied due to their application as nuclear materials [1–3]. The large energy deposition of swift heavy ions with GeV energies triggers, through intense excitation and ionization processes, complex material modifications that lead most commonly to amorphization (*e.g.*, $Y_3Fe_3O_{12}$ [4]), disordering (*e.g.*, $Gd_2Zr_{2-x}Ti_xO_7$ [5]), and formation of simple defects and/or defect clusters (*e.g.* ThO_2 [6]). In a limited number of materials, high-energy ions induce crystalline-to-crystalline structural transformations to high-temperature or high-pressure phases [7–17]. The most prominent examples are probably the monoclinic-to-tetragonal phase transformation in zirconia, ZrO_2, and hafnia, HfO_2 [7–14].

Rare earth sesquioxides (Ln_2O_3 with Ln = La through Lu) have a rich variety of phases as illustrated by their phase diagram (Fig. 1) with a number of crystalline polymorphs that form as a function of chemical composition, temperature, and pressure [18,19]. At ambient conditions, the hexagonal *A*-form ($P\bar{3}m1$) is the stable structure for rare earth cations with a large ionic radius (La ↔ Nd), while the cubic *C*-form ($Ia\bar{3}$) exists for smaller rare earth cations (Tb ↔ Lu). The intermediate compositions (Sm ↔ Gd) can be found either in the cubic *C*-form or in the monoclinic *B*-form ($C2/m$). At high temperature (2300–2500 K), all three polymorphs (*A*, *B*, and *C*) transform to the hexagonal *H*-form ($P6_3/mmc$). A second phase transition to the cubic *X*-form ($Im\bar{3}m$) can be induced at slightly higher temperatures of 2400–2700 K for compositions with cations larger than Dy (Fig. 1). Finally, all rare earth sesquioxides melt at even higher temperatures, with a melting temperature that increases slightly with decreasing cation ionic radius. Rare earth sesquioxides find applications in a wide range of technologies. For example, Gd_2O_3 has an enormous thermal-neutron absorption cross section and is an excellent "burnable poison" which is added to UO_2 nuclear fuel in order to improve reactor performance [20,21]. Due to the combination of magnetic and optical properties, doped and undoped gadolinium oxide is used in biomedical applications, for optical and magneto-resonance imaging [22–24].

Irradiation experiments with low-energy ions (keV), mostly at cryogenic temperatures, induce phase transformations in Dy_2O_3 and Er_2O_3 [25–27]. Tang and coworkers have shown by means of grazing incidence XRD and transmission electron microscopy that both sesquioxides undergo a *C*-to-*B* transformation with increasing fluence of 300 keV Kr ions [25]. At extremely high fluences in

---

[*] Corresponding author. Tel.: +1 865 974 8247.
E-mail address: mlang2@utk.edu (M. Lang).

http://dx.doi.org/10.1016/j.nimb.2013.10.073
0168-583X/© 2014 Elsevier B.V. All rights reserved.

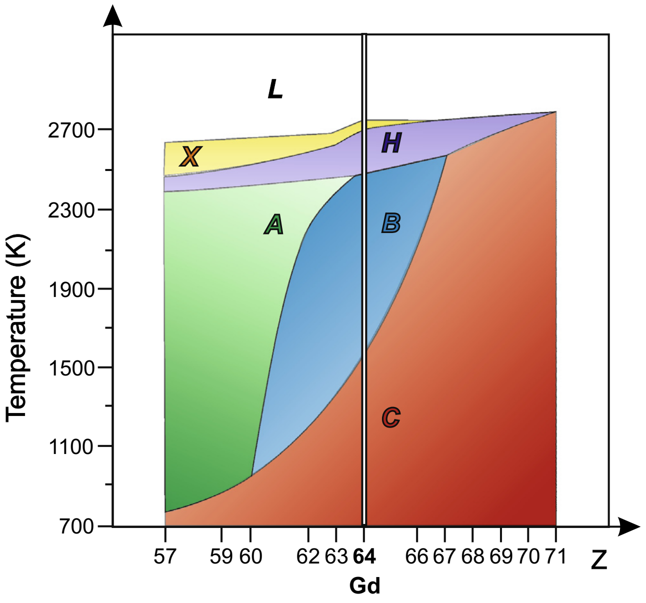

Fig. 1. Phase diagram for rare earth sesquioxides (Ln_2O_3) after Foex and Traverse [18] with respect to the atomic number of the cation. The different phases are A (hexagonal, $P\bar{3}m1$), B (monoclinic, $C2/m$), C (cubic, $Ia\bar{3}$), H (hexagonal, $P6_3/mmc$), X (cubic, $Im\bar{3}m$), and L denoting liquid (melt phase).

excess of 5×10^{16} Kr/cm^2, a partial *B*-to-*H* transformation was reported for Dy_2O_3 [26]. The radiation response of rare earth sesquioxides is not well studied with respect to swift heavy ions [16,17]. The polymorphism of Ln_2O_3 materials makes them ideal candidates for the investigation of ion-induced crystalline-to-crystalline transformations. In this paper we present a synchrotron XRD study of swift heavy ion irradiation damage in Gd_2O_3.

2. Experimental procedure

The ion irradiation of microgram Gd_2O_3 powder with a typical grain size on the order of a few µm and subsequent characterization by means of synchrotron XRD experiments required a new holder system. Microscopic sample chambers were prepared in a 50-µm thin stainless steel foil (Alfa Aesar, dimensions 2 × 20 mm^2) by drilling several holes with a diameter of 200 µm. A table-top electric discharge machining device from Hylozoic Micro EDM System equipped with a 200 µm copper wire was used to drill "through holes" in the steel foils by localized melting. After cleaning the sample chamber in an ultrasonic bath with acetone, Gd_2O_3 powder (MTI corporation, purity > 99.99 %) was placed over the holes and pressed between two steel die-pieces in a hydraulic laboratory press (MTI corporation) using a pressure of 20 MPa. Excess sample material was removed under the microscope to ensure well-defined sample-pellet dimensions of 200 µm in diameter and 50 µm in thickness (Fig. 2). Typically, seven small sample pellets (filled holes) were prepared in one steel holder for a given

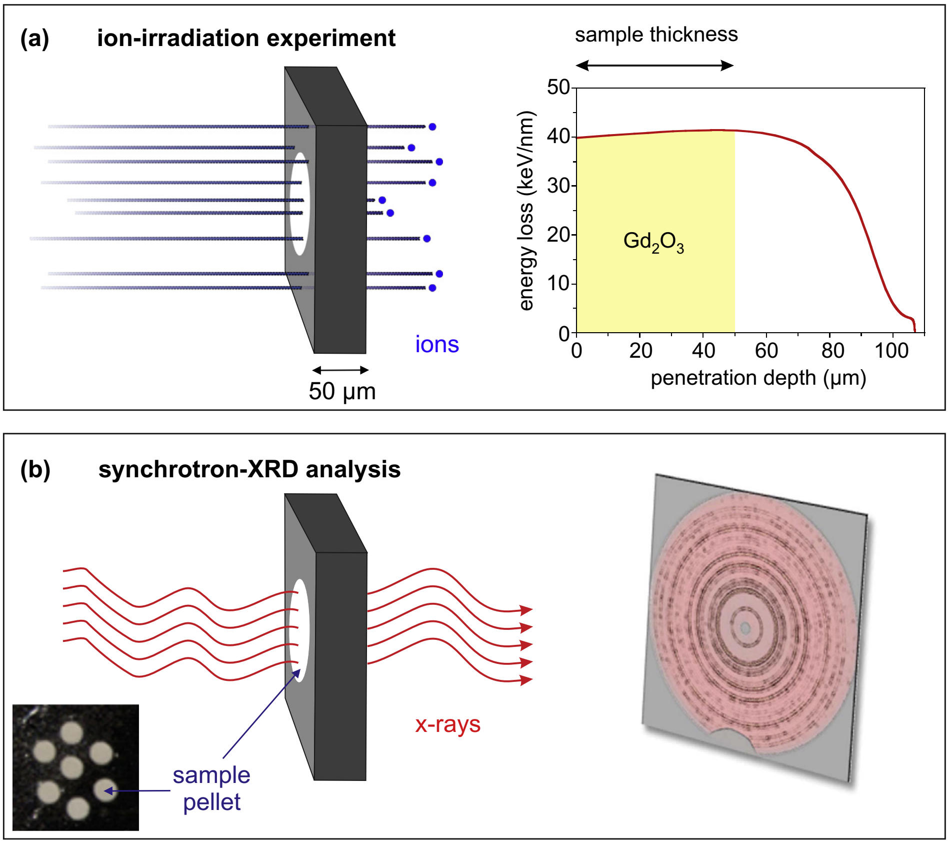

Fig. 2. Schematic of ion-irradiation experiment and synchrotron-XRD analysis. (a) Swift Au ions of 2.25 GeV kinetic energy completely penetrate the (white) powder sample pressed into a thin steel foil (diameter: 200 µm, thickness: 50 µm) inducing an almost constant energy loss of 40.8 keV/nm along their path. The spot size of the ion beam is significantly larger than the sample-pellet size. (b) Powder X-ray diffraction experiments with 30.5 keV X-rays (beam-spot diameter: 25 µm) from a synchrotron source are used to study ion-induced structural modifications throughout the sample thickness. The spot size of the X-ray beam is smaller than the sample-pellet size. Diffraction rings are recorded in transmission mode by a CCD detector. The photograph displays a steel holder with seven Gd_2O_3 sample pellets.

fluence, and ten sets of steel holders were irradiated at room temperature to fluences between 1×10^{10} and 5×10^{13} ions/cm^2. After the irradiation experiment and the transportation of samples between ion-accelerator and synchrotron facility, each steel holder was inspected under an optical microscope. Some sample pellets were partly or completely lost after irradiation and shipping. In cases where some of the sample was retained, Gd_2O_3 residue was present along the edges of the drilled holes. Apparently, the number of missing samples per steel holder increased with the ion fluence, and might thus be related mainly to irradiation-induced dimensional changes of the pellets, such as reduced volume due to densification. However, since seven pellets were prepared for each fluence, almost the entire fluence series could be analyzed by XRD measurements; only the holder exposed to the second highest fluence (2.5×10^{13} ions/cm^2) did not contain any sample. The irradiation experiment was completed with 2246 MeV Au ions at the M2 beamline of the UNILAC accelerator at the GSI Helmholtz Center for Heavy Ion Research in Darmstadt, Germany. The beam-spot size was about 1 cm^2, which covered all sample pellets in a given holder. The beam pulse had a length of 3 ms at 40 Hz and the flux did not exceed 5×10^9 ions/cm^2·s to avoid noticeable macroscopic sample heating.

With a theoretical density of 7.41 g/cm^3 for Gd_2O_3 oxide, the ion range was calculated to 64.4 µm using the SRIM-2013 code [28]. However, the actual density of the powder samples was significantly lower as compared with the theoretical value, since the pellets were prepared with a mechanical press operating at low pressure. In addition, the samples were not sintered after pressing. In a previous study on powdered actinide oxides cold pressing at 20 MPa resulted in an actual sample density that did not exceed 60% of the theoretical value [29]. To account for the reduced density of Gd_2O_3, the ion-range data from SRIM calculations, using the theoretical density, were multiplied by a factor of 1.66. The estimated penetration depth of the 2.25 GeV Au ions in powder pellets of about 60% density is at least 106 µm (Fig. 2a). The expected ion range is therefore more than 55 µm greater than the actual sample thickness. This approach was used instead of performing the SRIM calculations with reduced density because the loose packing of the sample pellets ("empty space") only increases the ion range, but did not decrease the dE/dx within the micrometer sized polycrystalline sample grains of theoretical density. The ions deposited an almost constant electronic energy loss of 40.8 keV/nm with a variation of ±1 keV/nm throughout the entire sample thickness [28] (Fig. 2a). The ion energy after the 50-µm thick pellets was reduced from 2246 MeV to about 1250 MeV based on the corrected range data. The nuclear energy loss is neglected because it is at least three orders of magnitude lower than the electronic energy loss.

Angle-dispersive synchrotron powder XRD measurements were performed as function of increasing fluence at the beam line X17C of the National Synchrotron Light Source, Brookhaven National Laboratory (monochromatic beam of about 30.5 keV and spot size ~25 µm). X-rays with a wavelength of 0.4082 Å were used in transmission mode to analyze ion-induced structural modifications throughout the entire sample (Fig. 2b). The measuring times were typically 5 min, but were optimized to gain maximum intensity and, thus, varied from sample to sample. The small sample pellets were initially aligned with respect to the X-ray beam with an optical microscope mounted at the beamline. Fine adjustment with accuracy at the µm-level was obtained by scanning the beam horizontally and vertically over the sample and monitoring its intensity with a photodiode. The center position of the sample pellet was located by the differences of X-ray absorption of sample and steel holder. Finally, horizontal scans at different angles were used to determine the position of the sample with respect to the rotation axis within 10 µm. Thus, the sample-detector distance was established with a very high accuracy (338.01 ± 0.01 mm). Debye diffraction rings were recorded with a Mar CCD detector, and the integrated two-dimensional patterns were produced with the software FIT2D [30]. The sample structure, including unit cell parameters, was derived from the refinement of the patterns using the Rietveld method with the program FullProf [31].

3. Results and discussion

Selected XRD patterns of Gd_2O_3 before and after irradiation with increasing fluence are shown in Fig. 3. Rietveld refinement of the pattern of the unirradiated sample confirmed the cubic (*C*-type) starting structure with a unit cell volume of $V = 1256.5(1)$ Å^3 and a unit cell parameter $a = 10.7907(7)$ Å in agreement with literature data [32]. No additional peaks from impurity phases or from the stainless steel holder were apparent in the pattern. Thus, the spot size of the focused X-ray beam (~25 µm) probed only the sample pellet (diameter: 200 µm). At a fluence of $\sim 2 \times 10^{12}$ ions/cm^2, a new sharp peak was detected in the pattern at a two theta position (~7.8°) slightly larger than the most intense (222) diffraction maximum of the cubic structure (~7.5°). With increasing fluence, several additional diffraction maxima appeared in the patterns that grew in intensity. The peaks of the cubic phase are all absent at the maximum fluence, indicating the complete transformation of the sample after irradiation with 5×10^{13} ions/cm^2. No evidence of amorphization was apparent in the diffraction patterns based on the absence of diffuse scattering bands at low two theta angles [5]. The complete phase transformation throughout the sample thickness confirms that the ions penetrated the entire 50-µm thick pellets. Previous irradiation experiments with swift heavy ions reported a transformation of cubic structured Y_2O_3 to the monoclinic *B*-type phase [16,17]. A simulated XRD pattern of monoclinic Gd_2O_3 using the software FullProf [31] is displayed in Fig. 3 (top pattern). This pattern is in

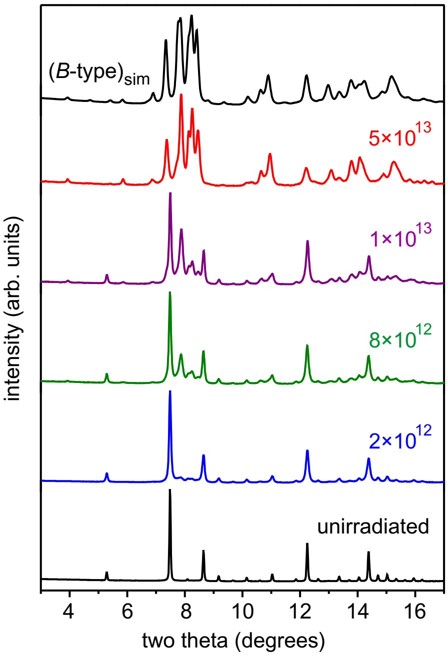

Fig. 3. Synchrotron X-ray diffraction patterns of Gd_2O_3 before and after irradiation with 2.25 GeV Au ions (fluence values are given in ions/cm^2). As function of increasing ion fluence (bottom to top), the initial cubic structure (*C*-type) gradually transforms to the monoclinic phase (*B*-type) as indicated by the appearance and growth of new diffraction maxima. At the maximum fluence of 5×10^{13} ions/cm^2, the transformation is complete and the XRD pattern agrees well with a simulated pattern of the monoclinic phase (*B*-type)$_{sim}$.

good agreement with the experimental results for the maximum fluence (second pattern from the top), confirming the same cubic-to-monoclinic phase transformation in gadolinium oxide induced by the 2.25 GeV Au ions. Despite the qualitatively good agreement of simulated and measured pattern, Rietveld refinement using a monoclinic Gd_2O_3 structural model ($C2/m$) [33] did not entirely reproduce the measured XRD patterns (not shown here). Minor deviations in peak intensity and position were evident. Relative changes in peak intensity can be explained by orientation effects, *i.e.*, preferred alignment of certain lattice planes with respect to the X-ray beam. However, the detector images from all of the samples consisted of continuous diffraction rings of constant intensity that is typical of synchrotron XRD data of powder samples with randomly oriented grains of size on the order of a few µm. The presence of an additional phase could also account for deviations in the XRD data from the pattern of a pure monoclinic phase. The *H*-type hexagonal high-temperature phase was previously reported to exist for Dy_2O_3 beyond the monoclinic structure after irradiation with 300 keV Kr ions to very high fluences of up to 5×10^{16} ions/cm^2 [26]. The present data for 2.25 GeV Au ions do not provide any evidence of the formation of a *H*-type phase. Thus, the origin of minor deviations of the experimentally obtained XRD patterns and the Rietveld refinement based on the ideal monoclinic structure are at present not resolved. They may be correlated to radiation effects in the monoclinic *B*-type structure, such as defects and associated microstrain [34], which are induced during (*i*) the formation process or (*ii*) the subsequent irradiation. This is supported by the increased peak width of the *B*-type phase.

Rietveld refinement was used in order to estimate the cubic and monoclinic sample fractions of the *C*-to-*B* transformation as function of fluence (Fig. 4). The ion-induced monoclinic structure forms at a relatively low fluence ($\sim 2 \times 10^{12}$ ions/cm^2) and increases initially only at a small rate, followed by a more pronounced increase above 6×10^{12} ions/cm^2 with a complete transformation at 5×10^{13} ions/cm^2. Despite the absence of data between 1×10^{13} and 5×10^{13} ions/cm^2, the initial behavior of the *C*-to-*B* transformation *vs.* fluence (Fig. 4) is not consistent with a single-ion impact mechanism, which is characterized by an initial linear increase followed by a sublinear reduction in the rate of phase transformation as a function of fluence, finally approaching saturation [35]. A single-impact mechanism was, however, found for the same cubic-to-monoclinic transformation in Y_2O_3 irradiated with swift heavy ions [17]. The present results for Gd_2O_3 suggest instead a multi-impact mechanism for the formation of the monoclinic phase, which is in good agreement with previous data on crystalline-to-crystalline phase transformations in other simple oxides [8,12–14,36]. For example, the swift heavy ion-induced phase transformation from monoclinic-to-tetragonal ZrO_2 was described with a double [8,12,13] and triple [14] ion-impact mechanism. The role of the first impact is associated with the creation of radiation defects, such as oxygen vacancies and related microstrain [12]. This has been confirmed by the behavior of ZrO_2 irradiated at various pressures up to 70 GPa with swift heavy ions [14,37]. The transformation efficiency to the tetragonal phase increased significantly if the simple oxide was under pressure during irradiation. The structural transition at high pressure may no longer require a double or triple impact process, because pressure induces an equivalent strain field within the sample. Since tetragonal zirconia and hafnia are high-temperature phases (formation temperature ~1400 and ~2000 K for ZrO_2 and HfO_2, respectively), it was also proposed that the phase transformation may be related to ion-induced thermal processes as described by the thermal-spike model [12,13]. This is consistent with the interpretation of the swift heavy ion-induced *C*-to-*B* transformation in Y_2O_3 [17]. Thermally induced processes may also play a role for Gd_2O_3 which has a comparable transition temperature. The *C*-to-*B* transformation starts above 1500 K (Fig. 1) and is completed at about 1670 K [21]. Once formed, the Gd_2O_3 monoclinic phase can be recovered to ambient conditions, while doping (*e.g.*, with Y) is required for the stabilization of zirconia high-temperature phases.

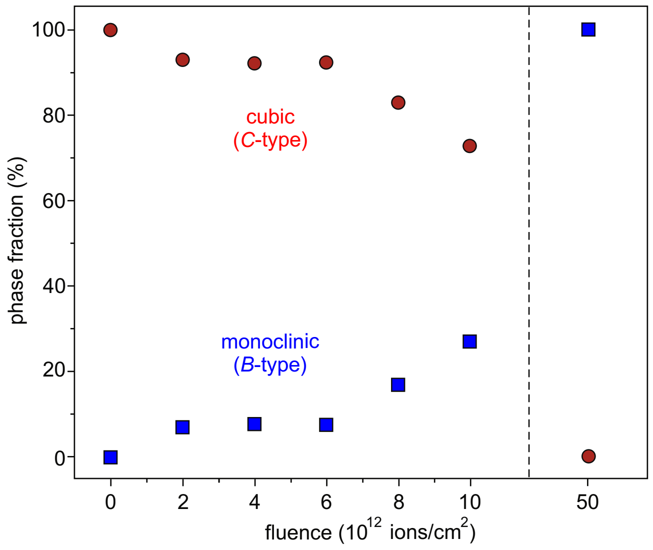

Fig. 4. Rietveld refinement results of synchrotron XRD patterns displaying the fraction of cubic (*C*-type, circles) and monoclinic (*B*-type, squares) structures as function of increasing ions fluence.

Under high pressure, the *C*-type Gd_2O_3 structure transforms irreversibly to an *A*-type hexagonal high-pressure phase between 7 and 15 GPa, which transforms to the *B*-type monoclinic structure after pressure release [38]. Thus, the final structural response under irradiation ($C \rightarrow B$) and high pressure ($C \rightarrow A \rightarrow B$) are identical. It is interesting to note that a very similar behavior has been previously reported for pyrochlore, which was attributed to the intrinsic energetics of defect formation under both irradiation and high pressure [39]. The formation of defects may also be crucial for ion-induced crystalline-to-crystalline transformations as indicated by Tang and co-workers [25]. They identified two possible coupled transformation mechanisms for the $C \rightarrow B$ transformation in Dy_2O_3 and Er_2O_3 after irradiation with low-energy ions [25]. The monoclinic phase forms (*i*) directly within a cascade by recrystallization from a thermal spike within some regions of the damage cascade, and (*ii*) indirectly through cascade overlap and accumulation of defects and defect cluster with an increase of the free energy. Irradiation-induced stress [25] and disordering to an anion-deficient fluorite structure [40] may be additional contributing factors. The distinct peak broadening in the XRD patterns of the initial cubic phase during the onset of the $C \rightarrow B$ transformation in Gd_2O_3 (Fig. 3) shows that defect accumulation and microstrain are similarly important for swift heavy ions. But in the case of swift heavy ions (electronic dE/dx), the transformation occurs at two orders of magnitude lower fluences as compared with low-energy ions (nuclear dE/dx) [25]. The increase of peak width can also originate from radiation-induced sample fragmentation. If a critical size is reached at the nanoscale, the $C \rightarrow B$ transformation may spontaneously occur since nanomaterials may exist in different phases as compared with their bulk counterparts due to the effect of surface energy and modified kinetics [41]. However, Gd_2O_3 exists as nanomaterial [23] and thin film [42] down to at least 10 nm in the cubic phase. The oxygen content has an important effect on the structure that forms, with the monoclinic phase being more preferred at lower oxygen concentrations [42,43]. Thus, a loss of oxygen during ion irradiation in a reducing environment (vacuum) may be another contributing factor for the $C \rightarrow B$ transformation. This may also account for the deviations from the ideal monoclinic structure as observed by the refinement. Finally, it is interesting to note that the $C \rightarrow B$ transformation involves an increase in atomic density by 9–10%, which is in contrast to the ion-induced swelling (*i.e.*, reduction in density) observed in most materials.

4. Conclusions

Polycrystalline samples of Gd_2O_3 sesquioxide were irradiated with 2.25 GeV Au ions in a newly developed sample holder system for microgram powdered samples. Characterization by means of synchrotron-based X-ray diffraction experiments, using the same holder systems, revealed an ion-induced crystalline-to-crystalline transformation. No amorphization was evident in the samples up to 5×10^{13} ions/cm^2. Rietveld refinement showed that the initial cubic structure transforms gradually to a monoclinic phase, which follows the behavior found in other cubic sesquioxides after ion irradiation. The phase transformation proceeds with swift heavy ions (electronic $dE/dx = 40.8$ keV/nm) at ambient temperature and can be induced at significantly lower fluences as compared with low-energy ion irradiations (nuclear dE/dx). The refinement results of the fraction of the phases as a function of fluence indicate that multiple swift heavy ions are required to trigger the structural transformation. Thermal effects, defects, strain, and changes in the oxygen content may all contribute to the transformation. The present results show that Gd_2O_3 within a nuclear environment, such as a burnable poison in UO_2-fuel, may undergo structural modifications due to exposure to fission fragments, which can result in significant changes in density.

Acknowledgements

The funding for this study was provided by the Office of Basic Energy Sciences of the USDOE (DE-FG02-97ER45656). The use of the National Synchrotron Light Source at X17C station is supported by NSF COMPRES EAR01-35554 and by US-DOE contract DE-AC02-10886. The authors gratefully acknowledge fruitful discussions with Dr. Marcel Toulemonde (Centre de recherches sur les Ions, les MAtériaux et la Photonique (CIMAP), Caen, France).

References

[1] K.E. Sickafus, L. Minervini, R.W. Grimes, J.A. Valdez, M. Ishimaru, F. Li, K.J. McClellan, T. Hartmann, Radiation tolerance of complex oxides, Science 289 (2000) 748.
[2] W.J. Weber, R.C. Ewing, Plutonium immobilization and radiation effects, Science 289 (2000) 2051.
[3] W.J. Weber, Alpha-irradiation damage in CeO_2, UO_2 and PuO_2, Radiat. Eff. 83 (1984) 145.
[4] M. Toulemonde, S. Bouffard, F. Studer, Swift heavy ions in insulating and conducting oxides: tracks and physical properties, Nucl. Instrum. Meth. B 91 (1994) 108.
[5] M. Lang, F.X. Zhang, J. Lian, C. Trautmann, Z. Wang, R.C. Ewing, Structural modifications of $Gd_2Zr_{2-x}Ti_xO_7$ pyrochlore induced by swift heavy ions: Disordering and amorphization, J. Mater. Res. 24 (2009) 1322.
[6] C.L. Tracy, J.M. Pray, M. Lang, D. Popov, C. Trautmann, R.C. Ewing, Defect accumulation in ThO_2 irradiated with swift heavy ions, Nucl. Instrum. Meth. B (2014), http://dx.doi.org/10.1016/j.nimb.2013.08.070.
[7] A. Benyagoub, F. Couvreur, S. Bouffart, et al., Phase transformation induced in pure zirconia by high energy heavy ion irradiation, Nucl. Instrum. Meth. B 175–177 (2001) 417.
[8] C. Gibert-Mougel, F. Couvreur, J.M. Constantini, S. Bouffard, et al., Phase transition of polycrysralline zirconia induced by swift heavy ion irradiation, J. Nucl. Mater. 295 (2001) 121.
[9] A. Benyagoub, Kinetics of the crystalline to crystalline phase transformation induced in pure zirconia by swift heavy ion irradiation, Nucl. Instrum. Meth. B 206 (2003) 132.
[10] A. Benyagoub, Evidence of an ion-beam induced crystalline-to-crystalline phase transformation in hafnia, Eur. Phys. J. B 34 (2003) 395.
[11] J.A. Valdez, M. Tang, Z. Chi, M.I. Peters, K.E. Sickafus, Characterization of an ion irradiation induced phase transformation in monoclinic zirconia, Nucl. Instrum. Meth. B 218 (2004) 103.
[12] A. Benyagoub, Mechanism of the monoclinic-to-tetragonal phase transition induced in zirconia and hafnia by swift heavy ions, Phys. Rev. B 72 (2005) 094114.
[13] A. Benyagoub, Phase transformations in oxides induced by swift heavy ions, Nucl. Instrum. Meth. B 245 (2006) 225.
[14] B. Schuster, F. Fujara, B. Merk, R. Neumann, T. Seidl, C. Trautmann, Response behavior of ZrO2 under swift heavy ion irradiation with and without external pressure, Nucl. Instrum. Meth. B 277 (2012) 45.
[15] H. Dammak, A. Barbu, A. Dunlop, D. Lesueur, N. Lorenzelli, $\alpha \rightarrow \omega$ phase transformation induced in titanium during ion irradiations in the electronic slowing-down regime, Philos. Mag. Lett. A 67 (1993) 253.
[16] S. Hémon, V. Chailley, E. Dooryhée, C. Dufour, F. Gourbilleau, F. Levesque, E. Paumier, Phase transformation of polycrystalline Y_2O_3 under irradiation with swift heavy ions, Nucl. Instrum. Meth. B 122 (1997) 563.
[17] S. Hémon, Ch. Dufour, F. Gourbilleau, E. Paumier, E. Dooryhée, S. Bégin-Colin, Influence of the grain size: yttrium oxide irradiated with swift heavy ions, Nucl. Instrum. Meth. B 146 (1998) 443.
[18] M. Foex, J.P. Traverse, Investigations about crystalline transformation in rare earths sesquioxides at high temperatures, Rev. Int. Hautes Temp. Refract. 3 (1966) 429.
[19] M. Zinkevich, Thermodynamics of rare earth sesquioxides, Prog. Mater Sci. 52 (2007) 597.
[20] F.B. Skogen, L.A. Nielsen, R.G. Grummer, Utilization of burnable poisons in LWRs operating experience with Exxon nuclear-supplied gadolinia in pressurized water reactors, Trans. Am. Nucl. Soc. 40 (1982) 194.
[21] M. Durazzo, F.B.V. Oliveira, E.F. Urano de Carvalho, H.G. Riella, The role of Gd_2O_3 phase transition on UO_2-Gd_2O_3 fuel sintering, J. Nucl. Mater. 400 (2010) 183.
[22] S. Seo, H. Yang, P.H. Holloway, Controlled shape growth of Eu- or Tb-doped luminescent Gd_2O_3 colloidal nanocrystals, J. Colloid Interface Sci. 331 (2009) 236.
[23] L. Zhou et al., Size-tunable synthesis of lanthanide-doped Gd_2O_3 nanoparticles and their applications for optical and magnetic resonance imaging, J. Mater. Chem. 22 (2012) 966.
[24] Y. Piao, A. Burns, J. Kim, U. Wiesner, T. Hyeon, Designed fabrication of silica-based nanostructured particle systems for nanomedicine applications, Adv. Funct. Mater. 18 (2008) 3745.
[25] M. Tang, P. Lu, J.A. Valdez, K.E. Sickafus, Ion-irradiation-induced phase transformation in rare earth sesquioxides (Dy_2O_3, Er_2O_3, Lu_2O_3), J. Appl. Phys. 99 (2006) 063514.
[26] M. Tang, P. Lu, J.A. Valdez, K.E. Sickafus, Heavy ion irradiation effects in the rare-earth sesquioxide Dy_2O_3, Nucl. Instrum. Meth. B 250 (2006) 142.
[27] B. Antic, A. Kremenovic, I. Draganic, Ph. Colomban, D. Vasiljevic-Radovic, J. Blanusa, M. Tadic, M. Mitric, Effects of O^{2+} ions beam irradiation on crystal structure of rare earth sesquioxides, Appl. Surf. Sci. 255 (2009) 7601.
[28] SRIM, 2013, http://www.srim.org/.
[29] E. Luther, C. Necker, B. Mihaila, P. Papin, D. Guidry, Microstructural characterization of uranium oxide, Trans. Am. Nucl. Soc. 104 (2011) 257.
[30] A.P. Hammersley, S.O. Svensson, M. Hanfland, A.N. Fitch, D. Häussermann, Two-dimensional detector software: from real detector to idealized image or two-theta scan, High Pressure Res. 14 (1996) 235.
[31] J. Rodríguez-Carvajal, FULLPROF 2000, version July 2001, Laboratoire Léon Brillouin (CEA-CNRS), France, 2001.
[32] B. Bartos, K.P. Lieb, M. Uhrmacher, D. Wiarda, Refinement of atomic positions in bixbyite oxides using perturbed angular correlation spectroscopy, Acta Crystallogr. B 49 (1993) 165.
[33] O.J. Guentert, R.L. Mozzi, The monoclinic modification of gadolinium sesquioxides Gd_2O_3, Acta Crystallogr. 11 (1958) 746.
[34] N. Paul, M. Devi, D. Mohanta, Synthesis, characterization and effect of low energy Ar ion irradiation on gadolinium oxide nanoparticles, Mater. Res. Bull. 46 (2011) 1296.
[35] W.J. Weber, Models and mechanisms of irradiation-induced amorphization in ceramics, Nucl. Instrum. Meth. 166 (2000) 98.
[36] J. Jagielski, L. Thomé, Multi-step damage accumulation in irradiated crystals, Appl. Phys. A 97 (2009) 147.
[37] B. Schuster, M. Lang, R. Klein, C. Trautmann, R. Neumann, A. Benyagoub, Structural phase transition in ZrO_2 induced by swift heavy ion irradiation at high-pressure, Nucl. Instrum. Meth. B 267 (2009) 142.
[38] F.X. Zhang, M. Lang, J.W. Wang, U. Becker, R.C. Ewing, Structural phase transitions of cubic Gd_2O_3 at high pressures, Phys. Rev. B 78 (2008) 064114.
[39] F.X. Zhang, J.W. Wang, J. Lian, M.K. Lang, U. Becker, R.C. Ewing, Phase stability and pressure dependence of defect formation in $Gd_2Ti_2O_7$ and $Gd_2Zr_2O_7$ pyrochlore, Phys. Rev. Lett. 100 (2008) 045503.
[40] M. Tang, J.A. Valdez, K.E. Sickafus, P. Lu, Order-disorder phase transformation in ion-irradiated rare earth sesquioxides, Appl. Phys. Lett. 90 (2007) 151907.
[41] C.T. Dameron, R.N. Reese, R.K. Mehra, A.R. Kortan, P.J. Carrol, M.L. Steigerwald, L.E. Brus, D.R. Winge, Biosynthesis of cadmium sulphide quantum semiconductor crystallites, Nature 338 (1989) 596.
[42] A. Molle, C. Wiemer, Md.N. Bhuiyan, G. Tallarida, M. Fanciulli, Cubic-to-monoclinic phase transition during the epitaxial growth of crystalline Gd_2O_3 films on Ge (001) substrates, Appl. Phys. Lett. 90 (2007) 193511.
[43] Y. Li, N. Chen, J. Zhou, S. Song, L. Liu, Z. Yin, C. Cai, Effect of the oxygen concentration on the properties of Gd_2O_3 thin films, J. Cryst. Growth 265 (2004) 548.